

# TAPE: Task-Agnostic Prior Embedding for Image Restoration

Lin Liu<sup>1</sup>   Lingxi Xie<sup>2</sup>   Xiaopeng Zhang<sup>2</sup>   Shanxin Yuan<sup>3</sup>  
Xiangyu Chen<sup>4</sup>   Wengang Zhou<sup>1</sup>   Houqiang Li<sup>1</sup>   Qi Tian<sup>2</sup>

<sup>1</sup>EEIS Department, University of Science and Technology of China

<sup>2</sup>Huawei Cloud BU

<sup>3</sup>Huawei Noah's Ark Lab

<sup>4</sup>University of Macau

**Abstract.** Learning an generalized prior for natural image restoration is an important yet challenging task. Early methods mostly involved hand-crafted priors including normalized sparsity,  $\ell_0$  gradients, dark channel priors, etc. Recently, deep neural networks have been used to learn various image priors but do not guarantee to generalize. In this paper, we propose a novel approach that embeds a task-agnostic prior into a transformer. Our approach, named Task-Agnostic Prior Embedding (TAPE), consists of three stages, namely, task-agnostic pre-training, task-agnostic fine-tuning, and task-specific fine-tuning, where the first one embeds prior knowledge about natural images into the transformer and the latter two extracts the knowledge to assist downstream image restoration. Experiments on various types of degradation validate the effectiveness of TAPE. The image restoration performance in terms of PSNR is improved by as much as 1.45 dB and even outperforms task-specific algorithms. More importantly, TAPE shows the ability of disentangling generalized image priors from degraded images, which enjoys favorable transfer ability to unknown downstream tasks.

## 1 Introduction

A good image prior can help to distinguish many kinds of noises from original image contents and improve the quality of images. Learning an image prior is important and challenging for image restoration tasks. Early studies explore specific degradation priors to achieve good performances on some low-level vision tasks, such as image dehazing [32,81], image deblurring [52,38], and image deraining [43,80]. However, most priors are hand-crafted and mainly based on limited observations. With the popularity of deep learning, data-driven image priors estimated by combining conventional degradation properties with deep neural networks have been explored [39,27,75,37,25,51,13]. But these networks capturing task-specific priors, do not guarantee to generalize to unseen tasks.

Recently, there are also efforts in learning complicated priors for low-level vision tasks [63,26,53,12,42,72]. These methods can be roughly grouped into two types. The first type [12,42] learns specific priors for each task, *i.e.*, the priors formulate ‘what is the distribution of specific noise’. Despite their effectiveness, these methods are often difficult to transfer across different tasks. The second

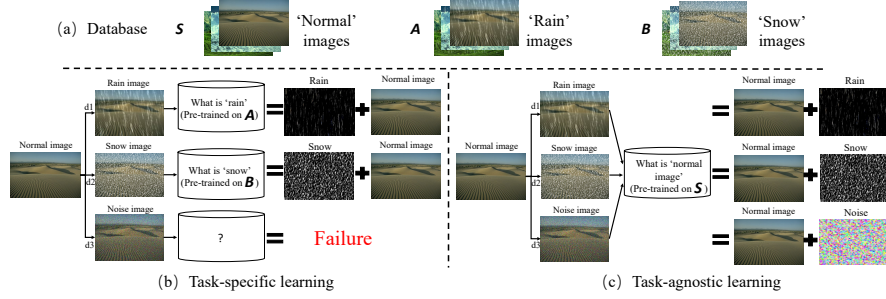


Fig.1: The illustration of the differences of task specific learning and task-agnostic learning. Our method aims to learn ‘what is normal image’ instead of ‘what are rain, snow or other degradation’.

type instead formulates generalized image priors, *i.e.*, ‘what is the distribution of normal images’. For this purpose, these methods [26,53,67] often make use of scalable GANs [6] pre-trained on natural images, hence, the learned priors are often hidden in a latent feature space, making it difficult to disentangle the noise from image contents, especially in the scenarios of complex images.

In this paper, we propose **Task-Agnostic Prior Embedding (TAPE)**, a novel kind of priors that are easily generalized to different low-level vision tasks. An intuitive comparison between TAPE and prior task-specific learning is illustrated in Fig. 1. TAPE absorbs the benefits of the aforementioned approaches: on the one hand, we learn the distribution of normal images from non-degraded natural images, which does not rely on any true or synthesized degradation; on the other hand, the priors are encoded in a simple prior learning module named PLM and the main network can decode them by transformer decoders (query embeddings). The training procedure of TAPE consists of three stages, namely, task-agnostic pre-training, task-agnostic fine-tuning, and task-specific fine-tuning, where a pixel-wise contrastive loss is designed in the first stage for unsupervised low-level representation learning.

In the experiment, we pre-train our model on four tasks (including deraining, deraindrop, denoising, and demoireing), fine-tune and test it on these four known tasks and four unknown tasks (desnowing, shadow removal, super-resolution, and deblurring). After the one-time learning, the generalized image prior (through pre-training) can be transferred to different tasks. To the best of our knowledge, it is the first work in this line of research. Quantitative and qualitative experimental comparisons show that the proposed TAPE improves the performance for multiple tasks in both task-specific and task-agnostic settings. In particular, our method improves the PSNR by 1.45dB, 1.03dB, 0.84dB, 0.49dB, and 0.75dB on the Rain200L, Rain200H, Raindrop800, SIDD, and TIP2018 datasets, respectively. The task-agnostic pre-training without touching the real noisy image on SIDD increases PSNR by 0.31dB. For the unseen tasks in the pre-training, TAPE improves the PSNR by 0.91dB, 0.29dB, 0.41dB and 0.48dB on desnowing, shadow removal, super-resolution, and deblurring, respectively.

In summary, the contributions of our work are:

- The possibility and importance of learning task-agnostic and generalized image prior is addressed. As far as we know, TAPE is the first work to (explicitly) represent the universal prior that can be used in multiple image restoration tasks. We disentangle the generalized clean image prior of the corrupted images from the degrading objects/noises.
- We propose a three-stage method named TAPE for image restoration to learn the generalized degradation prior.
- In the task-agnostic pre-training, we propose a pixel-wise contrastive loss for learning better generalized features for PLM. The combination of supervised and self-supervised training increase the generalization ability.

## 2 Related Work

**Image Restoration.** Image restoration is a general term for a series of low-level vision tasks, including denoising [74,76,28], deraining [43,80,41], deblurring [39,36], demoireing [62,78,30] *etc.* The aim of image restoration is to restore clean  $\mathbf{x}$  from corrupted  $\mathbf{y}$ . The corrupted image  $\mathbf{y}$  can be formulated as,  $\mathbf{y} = \mathbf{H}\mathbf{x} + \mathbf{v}$ , where  $\mathbf{H}$ ,  $\mathbf{x}$ , and  $\mathbf{v}$  are degradation matrix, underlying clean image, and noise, respectively. Before the deep learning era, studies design hand-crafted features of the degradation objects (*e.g.*, rain, snow, *etc.*) for different image restoration tasks. With the popularity of convolutional neural networks (CNNs), a handful of deep-learning based methods are proposed to handle one or multiple types of image restoration tasks. Most of these methods design task-specific models or loss functions to achieve better performances. For image super-resolution, Dong *et al.* propose SRCNN [21] to obtain high-resolution images from the corresponding low-resolution images. Fu *et al.* [24] introduce a ResNet-based CNN for image deraining. Li *et al.* and Yu *et al.*, propose FDRNet [42] and RL-Restore [72] to handle hybrid-distorted image restoration tasks. Zheng *et al.* [79] propose a learnable bandpass filter network for image demoireing. Different from these methods, we explore the power of pre-training to handle several image processing tasks.

**Image Degradation Prior and Natural Image Prior.** Since image restoration is ill-posed, the image prior can help to constrain the solution space. From the Bayesian perspective, the solution  $\hat{\mathbf{x}}$  can be obtained by optimizing:

$$\hat{\mathbf{x}} = \arg \min_{\mathbf{x}} \frac{1}{2} \|\mathbf{y} - \mathbf{H}\mathbf{x}\|^2 + \lambda \Phi(\mathbf{x}), \quad (1)$$

where the first term is the fidelity and the second term is the regularization. Deep-learning based methods try to learn the prior parameters  $\Theta$  and a compact inference through an optimization of a loss function on a training dataset with corrupted-clean image pairs. Then Eqn. 1 can be refined as,

$$\min_{\Theta} \ell(\hat{\mathbf{x}}, \mathbf{x}) \quad \text{s.t.} \quad \hat{\mathbf{x}} = \arg \min_{\mathbf{x}} \frac{1}{2} \|\mathbf{y} - \mathbf{H}\mathbf{x}\|^2 + \lambda \Phi(\mathbf{x}; \Theta). \quad (2)$$

Image priors have been widely used in computer vision, including markov random fields [60,82], dark channel prior [32,52], low rank prior [17], and total variation [61,3]. He *et al.* [32] propose dark channel prior for image dehazing. It exploits the prior property that in an haze-free image there are pixels where at least one color channel is of low value. Chen *et al.* [17] propose a low-rank model to capture the spatial and temporal correlations between rain streaks. Different from these task-specific priors, we use a pre-trained network to extract more general priors from images. The prior queries are also being adjusted during end-to-end training. Recently, deep image prior (DIP) [63] shows that image statistics can be implicitly captured by the network’s structure, which is also a kind of prior. Inspired by DIP, some attempts use a pre-trained GAN as a source of image statistics [26,53,58,23,10,67]. MGAN prior [26] utilizes multiple latent codes to increase the power of the pre-trained GAN model. DGP [53] fine-tunes the weights generator together with the latent code and use the discriminator to calculate the gap between the generated and real images.

**Image Restoration Transformers.** Transformer [64] is a new type of neural network framework of using mainly self-attention mechanism. It has been initially successfully used in natural language processing [20,7], such as BERT [20] and GPT-3 [7]. It has also been used in the computer vision field [22,8,47], such as vision transformer [22]. Transformers have achieved many successes in object classification [22], objection detection [83,19,9], *etc.* Very recently, it’s also been used in image restoration tasks [69,12,73,44,68,46,40]. Yang *et al.* [69] propose a texture transformer network for super-resolution, where the relevant textures are transferred from the reference images to low-resolution images. Chen *et al.* [12] and Li *et al.* [40] develop pre-trained transformers IPT and EDT respectively for three low-level vision tasks. Zeng *et al.* [73] proposes a spatial-temporal transformer network for video inpainting. We make use of the strong fitting ability of transformers and the learning ability of the transformer decoder to embed prior information.

### 3 Proposed Method

In this section, we first illustrate why we need to learn a task-agnostic prior (Sec. 3.1). And then, the architecture (Sec. 3.2) and the pipeline (Sec. 3.3) of our method are presented. At last, we briefly discuss the relationship to prior work (Sec. 3.4).

#### 3.1 Motivation

Most existing image restoration methods that train specific models for each single task (Fig. 1(b)) are difficult to generalize to new tasks. For example, a network trained on rain and no-rain image pairs will have difficulty dealing with denoising because of the different statistical characteristics of the degrading content. A better choice is to learn the natural image prior that is universal across multiple tasks. Thus, our work aims to design a pre-trained model that is suitable

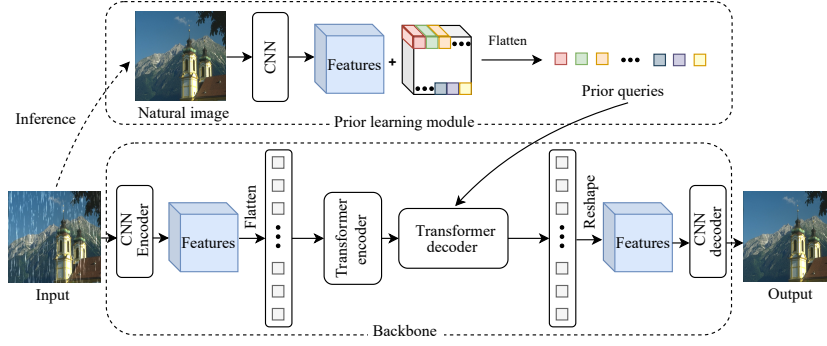


Fig. 2: The network architecture of our TAPE-Net. It consist of two parts: Backbone and prior learning module. With the input of natural images, PLM learns the features that natural images contain, not the features that noise contains. This makes our approach task-agnostic.

for various downstream image restoration tasks. For this purpose, the key is to learn **task-agnostic priors** and embed the priors into various tasks. Here, by task-agnostic, we hope the prior to indicate ‘what is a non-degraded (normal) image’ rather than ‘what is degradation’ which is task-specific (Fig. 1(c)). This is exactly what the prior learning module (PLM) is designed for – it extracts statistics from the normal (GT) images and uses the statistics to assist the main network for image restoration. With the task-agnostic embedding of PLM, our network is first pre-trained on natural images from multiple datasets, and can be easily refined to address any new image restoration task.

### 3.2 Network Architecture

The TAPE-Net (see Fig. 2) consists of two components: backbone and prior learning module. The backbone has a transformer architecture, containing a CNN encoder for feature extraction, a transformer encoder, a transformer decoder, and a CNN decoder for mapping the deep features into restored images. With the self-attention mechanism, the transformer can separate the generalized prior from the corrupted images. Different from conventional transformer, the decoder of our transformer takes additional prior queries, which comes from the prior learning module.

#### 3.2.1 Details of Network Architecture

**CNN encoder and CNN decoder.** The CNN encoder consists of two  $3 \times 3$  convolutional layers. The RGB image,  $I \in \mathbb{R}^{3 \times H \times W}$ , is the input of the CNN encoder, which generates a feature map  $f_e \in \mathbb{R}^{64 \times H \times W}$  with 64 channels and with the same resolution as  $I$ . The CNN decoder also consists of two  $3 \times 3$  convolutional layers. It generates a reconstructed image  $O \in \mathbb{R}^{3 \times H \times W}$ .

**Transformer encoder.** The feature map  $f_e$  is firstly flattened into small patches  $\{f_e^1, f_e^2, \dots, f_e^N\}$ , where  $f_e^i \in \mathbb{R}^{64P^2}$  ( $i = 1, 2, \dots, N$ ),  $N = \frac{HW}{P^2}$  is the total patch number and  $P$  is the patch size. A learnable position encoding  $PE_i$  with the same size of  $f_e^i$  is added to  $f_e^i$  and the sum (denoted as  $x_i$ ) is sent into the transformer encoder. The transformer encoder has  $n$  transformer blocks ( $n = 1$  in this work), each having a multi-head self-attention module and a feed forward network.

The process of the transformer encoder can be formulated as,

$$\begin{aligned} x' &= \text{MSA}(\text{LN}(x), \text{LN}(x), \text{LN}(x)) + x \\ o_e &= \text{FFN}(\text{LN}(x')) + x', \end{aligned} \quad (3)$$

where MSA, FFN, and LN denote the multi-head self-attention module, feed forward network, and linear layer in the conventional transformer [64], respectively.  $x = [x_1, x_2, \dots, x_N]$  and  $o_e = [o_{e1}, o_{e2}, \dots, o_{eN}]$  are the input and the output with the same size, respectively.

**Prior learning module.** The prior learning module (PLM) aims at providing additional prior queries to the transformer decoder. As shown in Fig. 2, PLM encodes an image into a feature map, and it can be formulated as  $f_n = G_n(I_{gt})$ , where  $f_n$  is a  $64 \times H \times W$  feature map representing the deep natural image features and  $G_n$  is a VGG19 network to extract image features. Then  $f_n$  is flattened into a series of patches  $[f_n^1, f_n^2, \dots, f_n^N]$  and combined with learnable parameters  $[e_1, e_2, \dots, e_N]$  as follows,

$$Q = [e_1 + f_n^1, e_2 + f_n^2, \dots, e_N + f_n^N], \quad (4)$$

where  $Q$  have the same length as  $o_e$ .

**Transformer decoder.** The transformer decoder has a similar architecture as the transformer encoder except for an additional input of the prior queries  $Q$ . In this paper, we use one transformer decoder block that consists of two multi-head self-attention (MSA) layers and one feed forward network (FFN). The transformer decoder is formulated as,

$$\begin{aligned} y &= \text{MSA}(\text{LN}(o_e) + Q, \text{LN}(o_e) + Q, \text{LN}(o_e)) + o_e \\ y' &= \text{MSA}(\text{LN}(y) + Q, \text{LN}(o_e), \text{LN}(o_e)) + y \\ o_d &= \text{FFN}(\text{LN}(y')) + y', \end{aligned} \quad (5)$$

where  $o_d = [o_{d1}, o_{d2}, \dots, o_{dN}]$  denotes the outputs of the transformer decoder. And then these patches are reshaped into  $f_d$  with the size of  $64 \times H \times W$ .

### 3.3 Optimization

#### 3.3.1 The Three-Stage Pipeline

From Sec. 3.2.1, in our network design, PLM should extract statistics from the non-degraded (Ground truth) image and use the statistics to assist the main network for image restoration. However, ground truth is unavailable during the inference (test) stage. So PLM cannot extract statistics from it. To compensate, we train an auxiliary module (backbone  $\phi$  in Fig. 3) to generate a pseudo

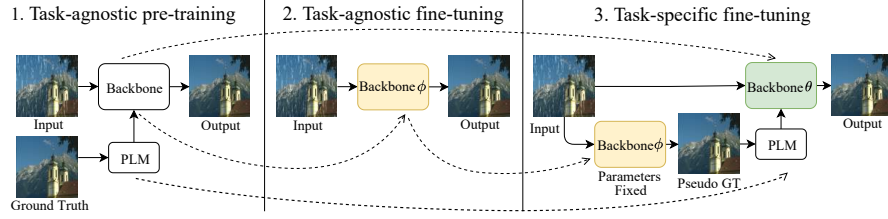


Fig. 3: The procedure of TAPE. TAPE contains 3 stages: task-agnostic pre-training, task-agnostic fine-tuning and task-specific fine-tuning. The dotted line means that the network trained in the previous stage is used to initialize the network in the next stage.

GT from the degraded input. The pseudo GT, not being perfect, depicts the property of a non-degraded image to some extent. The pseudo GT is then fed into PLM for extracting task-agnostic priors, and the priors assist the main network (backbone  $\theta$ ) to generate the final output. As shown in Fig. 3, TAPE-Net has three stages: task-agnostic pre-training, task-agnostic fine-tuning, and task-specific fine-tuning.

In the task-agnostic pre-training, multiple low-level vision tasks are trained together, using corresponding datasets  $\{D_1, \dots, D_m\}$ , where  $D_i$ , ( $i = 1, 2, \dots, m$ ) represents the dataset for task  $i$ . In each iteration, a pair of images (a corrupted image  $I_{cor}$  and its ground truth  $I_{gt}$ ) are selected from one dataset  $D_i$ . The ground truth  $I_{gt}$  is sent into PLM to learn the prior queries, which are then sent to the backbone for end-to-end training. The combination of the  $L_1$  loss and the proposed pixel-wise contrastive loss (see section 3.3.2) is used to optimize the network (the weighting parameter is for the latter). Due to the task-agnostic pre-training, both the backbone network and the learnable parameters (see section 3.2.1) are well optimized, and the learnable parameters encode the image prior.

In the task-agnostic fine-tuning, we borrow the pre-trained backbone from the first stage which can serve as an auxiliary module (backbone  $\phi$  in Fig. 3) for the final stage to generate a pseudo GT from the degraded input (Note that the network used in this stage can be any neural network. For faster convergence, we use the network pre-trained in the first stage.). The backbone network is then further fine-tuned on all datasets. After this stage, the updated backbone network is denoted as ‘Backbone  $\phi$ ’ in the task-specific fine-tuning.

The task-specific fine-tuning takes both the weights of the backbone networks from the previous two stages. For each task, only the corresponding dataset is used in this stage. As shown in the right part of Fig. 3, the weights of ‘backbone  $\theta$ ’ and ‘backbone  $\phi$ ’ are from the backbones in the task-agnostic pre-training and task-agnostic fine-tuning, respectively. The ‘Backbone  $\phi$ ’ is fixed and used to estimate a pseudo ground truth, which is sent into PLM. With the estimated pseudo ground truth, PLM can capture the natural image priors better.

### 3.3.2 Pixel-wise Contrastive Loss

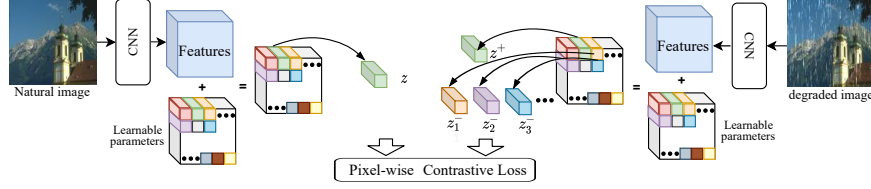


Fig. 4: The use of pixel-wise contrastive loss.  $z$  is selected from the prior queries of the natural image as ‘query’. And  $z^+$  and  $z_j^-$  are selected as the ‘positive’ and ‘negative’ elements in the contrastive loss, respectively.

PLM aims to estimate the distribution of natural patches. However, due to the limited amount of training data, learning from single patches (unary term) is insufficient for accurate estimation. Inspired by some self-supervised learning for high-level semantics (*e.g.* MoCo [31] and SimCLR [14]) and image to image translation method [4,54], we propose a pixel-wise contrastive loss to offer another cue (binary terms) of estimation – the distance between the features of  $I_d$  and  $I_{gt}$  (from the same location) shall be smaller than that between features from different locations.

As shown in Fig. 4, in the task-agnostic pre-training stage, the degraded image  $I_d$  and the natural image  $I_{gt}$  are put into PLM, then  $Q^d$  and  $Q^{gt}$  are obtained as described in Sec. 3.2. We aim at minimizing the distance between the features of  $I_d$  and  $I_{gt}$  from the same location while maximizing the distance between features from different locations. For example, in Fig. 4, the roof without rain should be more closely associated with the roof contaminated by the rain than the other patches of the rainy input, such as other parts of the house or the blue sky.

Suppose that  $q_i^d$  is selected from  $Q^d = \{q_1^d, q_2^d, \dots, q_N^d\}$  as the ‘query’ element in the contrastive loss.  $q_i^{gt}$  and  $q_{j_1}^{gt}, q_{j_2}^{gt}, \dots, q_{j_m}^{gt}$  are selected from  $Q^{gt} = \{q_1^{gt}, q_2^{gt}, \dots, q_N^{gt}\}$  as the ‘positive’ and ‘negative’ elements in the contrastive loss, respectively.

Thus, the contrastive loss is formulated as,

$$\mathcal{L} = \sum_{t=1}^T \ell_t(q_i^d, q_i^{gt}, q_j^{gt}), \quad (6)$$

$$\ell(q_i^d, q_i^{gt}, q_j^{gt}) = -\log \left[ \frac{\exp(q_i^d \cdot q_i^{gt} / \tau)}{\exp(q_i^d \cdot q_i^{gt} / \tau) + \sum_{k=1}^m \exp(q_i^d \cdot q_{j_k}^{gt} / \tau)} \right], \quad (7)$$

where  $T = 256$  is the feature number we randomly choose each time and the temperature  $\tau$  is set to 0.07. The negative sample number  $m$  is set to 256 in our work.

Table 1: Datasets’ statistics (number of training and testing images) and quantitative comparison for two models (in terms of PSNR (dB)).

Dataset	Rain200L	Rain200H	Raindrop800	SIDD	TIP2018	Snow100K	ISTD	DIV2K	REDS
#Train/test images	1800/200	1800/200	800/60	96000/1280	10000/200	10000/500	1330/540	800/100	24000/3000
Baseline	31.72	22.81	26.85	37.41	26.77	25.42	26.28	31.25	32.46
TAPE-Net (Ours)	33.17	23.84	27.69	37.90	27.52	26.33	26.57	31.66	32.94
PSNR Gain	+1.45	+1.03	+0.84	+0.49	+0.75	+0.91	+0.29	+0.41	+0.48

### 3.4 Relationship to Prior Work

1) Compared with recent multiple degradation prior learning methods (e.g., IPT and EDT), our TAPE formulates generalized image priors, which means that our method can generalize well to the pre-training-unknown tasks. 2) Different from the methods [26,53,5,67] where the learned image priors are hidden in the parameters of the generator, the learned prior of our model is explicit. It makes easy for our method to disentangle the unwanted noise from the image contents in some complex image restoration cases.

## 4 Experiments and Analysis

In this section, we evaluate the performance of TAPE on several low-level vision tasks and conduct an ablation study.

### 4.1 Tasks and Datasets

For pre-training, we use five datasets, each for one type of degradation. We also test on four more datasets for four tasks that are unknown in the pre-training stage. For both training and testing, we resize images into the resolution of  $256 \times 256$ , and then crop them into  $64 \times 64$  patches for balancing the training procedure with different data sizes. Note that same resizing and cropping operations are also adopted for other models for a fair comparison. The evaluated tasks include denoising, deraining, deraindrop, demoreing, desnowing, shadow removal, super resolution and deblurring. As shown in Table S1 for details, the used datasets are: SIDD [1] for denoising, Rain200H and Rain200L [71] for deraining, Raindrop800 [55] for deraindrop, TIP2018 [62] for demoreing<sup>1</sup>, Snow100K [48] for desnowing, ISTD [65] for shadow removal, DIV2K [2] for super resolution and REDS [50] for deblurring.

### 4.2 Implementation Details

**Pre-training.** We use one Nvidia Tesla V100 card to train our model using the Adam optimizer for  $60 \times 24000$  iterations on the mixture of the five dataset

<sup>1</sup> We select a subset of the TIP2018 dataset [62] with 10000 training image pairs and 200 test pairs.

Table 2: Quantitative comparison with the state-of-the-art deraining methods on Rain200L and Rain200H. The best result are in **Bold**.

Dataset	Method	DDN [24]	SPANet [66]	RESCAN [41]	PreNet [57]	BRN [56]	PCNet [34]	TAPE-Net (Ours)
Rain200L	PSNR/SSIM	28.35/0.878	30.92/0.930	32.07/0.949	31.98/0.948	32.40/0.953	32.62/0.954	<b>33.17/0.959</b>
Rain200H	PSNR/SSIM	20.98/0.705	22.65/0.714	23.04/0.729	23.27/0.743	23.39/0.755	23.43/0.755	<b>23.84/0.759</b>

Table 3: Quantitative comparison with the state-of-the-art dermoireing methods on TIP2018. The best result are in **Bold**.

Method	DMCNN [62]	MopNet [30]	HRDN [70]	FHDe2Net [29]	WDNet [45]	MBCNN [79]	TAPE-Net (ours)
PSNR/SSIM	25.82/0.806	26.20/0.861	26.68/0.864	26.25/0.862	26.86/0.865	27.37/0.866	<b>27.52/0.866</b>

(SIDD, Rain200L, Rain200H, Raindrop800, and TIP2018). The initial learning rate is set as 0.0002 and decayed to 0.0001 in the  $20 \times 24000$ th iteration with batch size 4. In each iteration, we first randomly choose a dataset, from which one clean-corrupted image pair is randomly selected.

**Fine-tuning.** After pre-training on all the datasets, we fine-tune the model on each desired task (*e.g.*, denoising). TAPE-Net is fine-tuned with 200 epochs and a learning rate of  $2e-4$  for both task-agnostic and task-specific fine-tuning.

### 4.3 Pre-training & Generalization Ability

In this subsection, we illustrate that our method has good generalization performance on both pre-training-known tasks and pre-training-unknown tasks.

**Pre-training-known tasks, corresponding data.** To illustrate the effectiveness of our task-agnostic pre-training, we compare our pre-trained model with the model without pre-training (denoted as ‘Baseline’ in Table S1). The TAPE-Net improve the PSNR by 1.45dB, 1.03dB, 0.84dB, 0.49dB and 0.75dB on the Rain200L, Rain200H, Raindrop800, SIDD, and TIP2018 dataset, respectively. Please note that in image restoration, an 0.5dB improvement is usually considered significant. It demonstrates the effectiveness of the pre-training and the superiority of our model.

**Pre-training-known tasks, different data.** And we also do experiments to explore the good generalization performance of our pre-trained model when transferred to different distributions of data in the pre-training-known task. Our experiments show that pre-training with synthetic Gaussian noises helps to restore the images corrupted by real noises (see Table 4). In practice, in the task-agnostic pre-training, we use ground truth in SIDD with added synthetic Gaussian noises as input, without touching the real noise images on the SIDD dataset. Then the pre-trained model is fine-tuned on SIDD (using real-noise/non-noise image pairs). The PSNRs increase by 0.19dB, and 0.31dB respectively when the  $\sigma$  of the added Gaussian noise (Sampled from  $\mathcal{N}(0, \sigma)$ ) are in [5,20], and

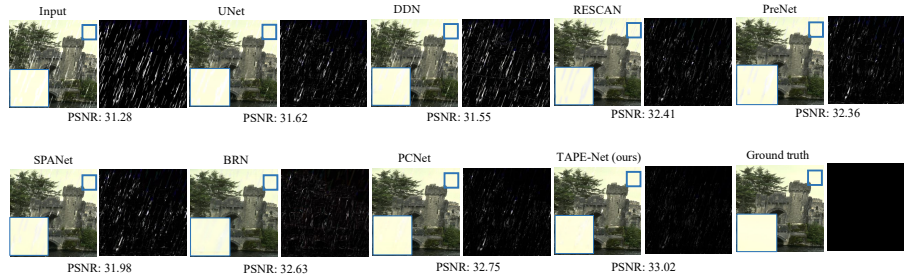


Fig. 5: Visual deraining comparison among our methods and SOTA deraining methods on Rain200L. The second and the last rows are the differences between the output and the ground truth.

[1,50], respectively. When the range of the added Gaussian noise is larger, the generalization ability of the model in the pre-training stage is stronger, and the performance in the fine-tuning stage is better.

**Pre-training-unknown tasks.** To illustrate the generalization ability of our model, we conduct several experiments on the tasks that are unknown to the pre-training stage. In practice, we fine-tune the pre-trained model on four new low-level vision tasks: desnowing, shadow removal, super resolution and deblurring. As shown in Table S1, compared with the none-pre-trained model, TAPE-Net improves the PSNR by 0.91dB, 0.29dB, 0.41dB and 0.48dB, which demonstrates that the pre-trained model can capture more useful information and features from natural images. Learning task-agnostic priors and pixel-wise contrastive loss on pre-training stage can help the performance of fine-tuning on the unknown tasks.

#### 4.4 Comparisons with State-of-the-Arts

In this section, we compare our TAPE-Net with 12 state-of-the-art methods, including DDN [24], SPANet [66], RESCAN [41], PreNet [57], PCNet [34], BRN [56], DMCNN [62], MopNet [30], FHDe2Net [30], HRDN [70], WDNNet [45] and MBCNN [79]<sup>2</sup>. As shown in Table 2, we compare our TAPE-Net with some deraining-specific methods on Rain200L and Rain200H. Our methods outperform all the deraining methods by at least 0.55 dB and 0.41 dB, respectively. Qualitative results are compared in Figs. 5 and 6, showing that our methods get cleaner images and recover more details. We also compare with several state-of-the-art demoiring-specific methods on TIP2018 dataset (see Table 3). Note that all methods are tested on the selected subset for fair comparison. Our methods outperform these demoiring specific methods by at least 0.15dB. The visual results are shown in Fig. 7. Ours can remove the moire patterns successfully and restore the underlying clean image. The comparison between our methods and

<sup>2</sup> See the supplementary materials for more descriptions and results.

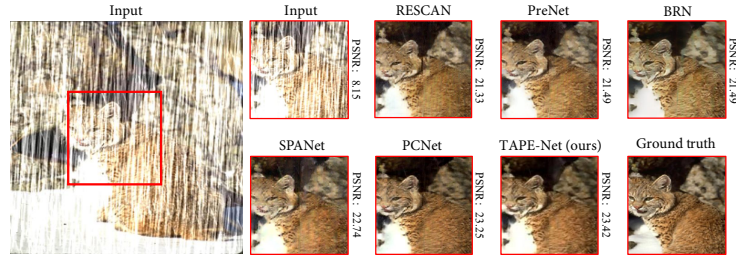


Fig. 6: Visual deraining comparison among our methods and some SOTA de-raining methods on Rain200H. Our method can remove the rain streaks more thoroughly and retain more details.

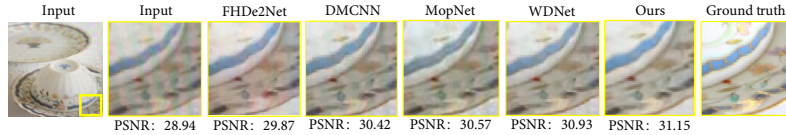


Fig. 7: Visual comparison among our methods and SOTA demoireing methods on TIP2018.

the general methods which are widely used in image restoration (*e.g.*, U-Net) is shown in the supplementary materials.

In order to show the advantage of our method on pre-training-unknown tasks, we compare ours with the existing SOTA multi-task pre-training method, IPT [12]<sup>3</sup>. We fine-tuned and tested the official pre-trained model of IPT on three unseen tasks, namely, desnowing, shadow removal and deblurring. For fair comparison, we compared the gain of PSNR with and without pre-training, because the training patches of IPT and ours are different. The pre-training stage of IPT boosts PSNR by 0.07dB, 0.19dB and 0.08dB, respectively, while the improvements of TAPE (our method) are 0.91dB, 0.29dB and 0.48dB, larger than that of IPT.

#### 4.5 Ablation Study

**Impact of the multi-task pre-training.** We do ablation study to analyze the effect of the number of datasets in the pre-training. We pre-train our models on fewer datasets and compare with our original models. As shown in Table 5, RD, TIP, RL, RH, and S mean Raindrop800, TIP2018, Rain200L, Rain200H, and SIDD datasets respectively. ‘+’ means we use these datasets in the pre-training stage. We do the experiments on three pre-trained-known datasets and the maximum PSNR difference is 0.04 dB. This PSNR difference is within a

<sup>3</sup> The code and the pre-trained model of EDT [40] are not released, thus we do not compare with it.

Table 4: Quantitative comparison on SIDD. It shows the good generalization performance of TAPE-Net when transferred to different distributions of data in the pre-training-known task.

TAPE-Net	W/o pre-train	Pre-train ( $\sigma \in [5,20]$ )	Pre-train ( $\sigma \in [1,50]$ )
PSNR	37.41	37.60	37.72

Table 5: Ablation study of the impact of the multi-task pre-training and the task-specific fine-tuning. The first part illustrates that adding more tasks will not harm the performance. The second part shows that the task-specific fine-tuning enhances the results.

	Raindrop800	Rain200L	TIP2018	Snow100K
RD+RL+RH	27.71	33.20	27.56	26.17
RD+TIP+RL+RH	27.70	33.18	27.54	26.26
W/o TS Fine-tuning	27.05	32.86	27.01	25.63
The whole pipeline*	27.69	33.17	27.52	26.33

\* The whole pipeline is pre-trained using five datasets (RD, TIP, RL, RH, and S).

controllable error range. Increasing the dataset in the pre-training is meaningful. Compared with pre-training with 3 datasets, pre-training with 5 datasets increases the PSNR by 0.16dB on Snow100K.

**The task-specific fine-tuning of TAPE-Net.** To verify the contributions of the task-specific fine-tuning stage of TAPE-Net, we conduct an ablation study on the Deraindrop800, Rain200L, and TIP2018 datasets. In the last two rows of Table 5, ‘W/o TS Fine-tuning’ means we remove the task-specific fine-tuning stage in the original pipeline and the outputs of the task-agnostic fine-tuning are served as the final results. ‘The whole pipeline’ means the original pipeline of TAPE-Net. As shown in Table 5, ‘W/o TS Fine-tuning’ decreases the PSNR by 0.64dB, 0.31dB, and 0.51dB respectively, which shows that the task-specific fine-tuning stage in TAPE-Net is important.

**Importance of pre-training of each component.** In order to prove that the prior learning module (PLM), not the backbone, learns the natural image priors in the task-agnostic pretraining, we randomize the weights of backbone of TAPE-Net before the fine-tuning stages. The first line in Table 6 shows that this operation achieves also the same effect as the original method. And we also randomize the weights of the whole TAPE-Net before the fine-tuning stages. The PSNR/SSIM decrease by 0.4dB/0.004, which means that the performance of our method deteriorates when PLM is not pre-trained.

**Importance of pixel-wise contrastive loss.** We remove the pixel-wise contrastive loss in the task-agnostic pretraining. As shown in the 3rd line of Table

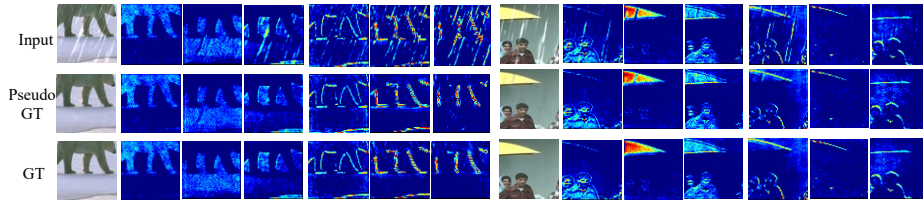


Fig. 8: The visualization of the PLM’s output,  $Q$ . The features of the pseudo GT and GT are very similar, but most of the features of input have the features of degraded objects. It means that the features of the pseudo GT is useful and can help the image restoration of the backbone.

C & T Encoder	C & T Dncoder	PLM	C Loss	PSNR	SSIM
-	-	✓	✓	33.14	0.958
-	-	-	✓	32.77	0.955
✓	✓	✓	✓	33.05	0.958
✓	✓	✓	✓	<b>33.17</b>	<b>0.959</b>

Table 6: The ablation study of the importance of each pre-trained part, pixel-wise contrastive loss on the Rain200L dataset. ‘-’ in the first three columns means that the model parameters are randomized before the fine-tuning.

6, The PSNR/SSIM decrease by 0.12dB/0.001 without the proposed pixel-wise contrastive loss.

#### 4.6 Visualization Results

To validate that PLM learns useful and meaningful features with our proposed pipeline, we visualize the features learned by PLM on the deraining task. We put the input, pseudo GT and GT into PLM to get their respective output  $Q$ . As shown in Fig. 8, in the output features, some channels tend to preserve the information of shapes (the first three feature maps) and edges (the last three feature maps). The features of the pseudo GT and GT are very similar, but most of the features of input have the features of degraded objects. It means that the features of the pseudo GT is useful and can help the image restoration of the backbone. In the supplementary material, we show that PLM can associate the information of similar textures or patches from a long distance.

## 5 Conclusions

In this paper, we propose a pipeline named TAPE to learn task-agnostic prior embedding for image restoration. TAPE has three stage: task-agnostic pre-training, task-agnostic fine-tuning and task-specific fine-tuning. Our task-mixture

training strategy is able to learn generalized natural image prior. It has good generalization performance when faced with pre-training-unknown tasks. The three-stage pipeline may make the training time longer than the baseline. And the performance of TAPE on mixed degradation tasks needs to be explored.

## References

1. Abdelhamed, A., Lin, S., Brown, M.S.: A high-quality denoising dataset for smart-phone cameras. In: CVPR, 2018
2. Agustsson, E., Timofte, R.: Ntire 2017 challenge on single image super-resolution: Dataset and study. In: CVPRW, 2017
3. Babacan, S.D., Molina, R., Katsaggelos, A.K.: Variational bayesian blind deconvolution using a total variation prior. TIP, 2008
4. Baek, K., Choi, Y., Uh, Y., Yoo, J., Shim, H.: Rethinking the truly unsupervised image-to-image translation. In: International Conference on Computer Vision (ICCV, 2021)
5. Bau, D., Strobel, H., Peebles, W., Zhou, B., Zhu, J.Y., Torralba, A., et al.: Semantic photo manipulation with a generative image prior. arXiv preprint arXiv:2005.07727 (2020)
6. Brock, A., Donahue, J., Simonyan, K.: Large scale gan training for high fidelity natural image synthesis. In: ICLR, 2018
7. Brown, T.B., Mann, B., Ryder, N., Subbiah, M., Kaplan, J., Dhariwal, P., Neelakantan, A., Shyam, P., Sastry, G., Askell, A., et al.: Language models are few-shot learners. arXiv preprint arXiv:2005.14165, 2020
8. Carion, N., Massa, F., Synnaeve, G., Usunier, N., Kirillov, A., Zagoruyko, S.: End-to-end object detection with transformers. In: ECCV, 2020
9. Carion, N., Massa, F., Synnaeve, G., Usunier, N., Kirillov, A., Zagoruyko, S.: End-to-end object detection with transformers. In: ECCV, 2020
10. Chan, K.C., Wang, X., Xu, X., Gu, J., Loy, C.C.: Glean: Generative latent bank for large-factor image super-resolution. arXiv preprint arXiv:2012.00739 (2020)
11. Chang, M., Li, Q., Feng, H., Xu, Z.: Spatial-adaptive network for single image denoising. ECCV, 2020
12. Chen, H., Wang, Y., Guo, T., Xu, C., Deng, Y., Liu, Z., Ma, S., Xu, C., Xu, C., Gao, W.: Pre-trained image processing transformer. CVPR, 2021
13. Chen, L., Fang, F., Wang, T., Zhang, G.: Blind image deblurring with local maximum gradient prior. In: CVPR, 2019
14. Chen, T., Kornblith, S., Norouzi, M., Hinton, G.E.: A simple framework for contrastive learning of visual representations. In: ICML, 2020
15. Chen, W.T., Fang, H.Y., Ding, J.J., Tsai, C.C., Kuo, S.Y.: Jstasr: Joint size and transparency-aware snow removal algorithm based on modified partial convolution and veiling effect removal. In: ECCV, 2020
16. Chen, W.T., Fang, H.Y., Hsieh, C.L., Tsai, C.C., Chen, I., Ding, J.J., Kuo, S.Y., et al.: All snow removed: Single image desnowing algorithm using hierarchical dual-tree complex wavelet representation and contradict channel loss. In: CVPR, 2021
17. Chen, Y.L., Hsu, C.T.: A generalized low-rank appearance model for spatio-temporally correlated rain streaks. In: ICCV, 2013
18. Cun, X., Pun, C.M., Shi, C.: Towards ghost-free shadow removal via dual hierarchical aggregation network and shadow matting gan. In: AAAI, 2020

19. Dai, Z., Cai, B., Lin, Y., Chen, J.: Up-detr: Unsupervised pre-training for object detection with transformers. In: CVPR, 2021
20. Devlin, J., Chang, M.W., Lee, K., Toutanova, K.: Bert: Pre-training of deep bidirectional transformers for language understanding. arXiv preprint arXiv:1810.04805 (2018)
21. Dong, C., Loy, C.C., He, K., Tang, X.: Image super-resolution using deep convolutional networks. TPAMI, 2015
22. Dosovitskiy, A., Beyer, L., Kolesnikov, A., Weissenborn, D., Zhai, X., Unterthiner, T., Dehghani, M., Minderer, M., Heigold, G., Gelly, S., et al.: An image is worth 16x16 words: Transformers for image recognition at scale. arXiv preprint arXiv:2010.11929, 2020
23. El Helou, M., Ssstrunk, S.: BIGPrior: Towards decoupling learned prior hallucination and data fidelity in image restoration. arXiv preprint arXiv:2011.01406 (2020)
24. Fu, X., Huang, J., Zeng, D., Huang, Y., Ding, X., Paisley, J.: Removing rain from single images via a deep detail network. In: CVPR, 2017
25. Golts, A., Freedman, D., Elad, M.: Unsupervised single image dehazing using dark channel prior loss. TIP, 2020
26. Gu, J., Shen, Y., Zhou, B.: Image processing using multi-code gan prior. In: CVPR, 2020
27. Guo, S., Liang, Z., Zhang, L.: Joint denoising and demosaicking with green channel prior for real-world burst images. arXiv preprint arXiv:2101.09870 (2021)
28. Guo, S., Yan, Z., Zhang, K., Zuo, W., Zhang, L.: Toward convolutional blind denoising of real photographs. In: CVPR, 2019
29. He, B., Wang, C., Shi, B., Duan, L.Y.: Fhde2net: Full high definition demoireing network. ECCV, 2020
30. He, B., Wang, C., Shi, B., Duan, L.Y.: Mop moire patterns using mopnet. In: ICCV, 2019
31. He, K., Fan, H., Wu, Y., Xie, S., Girshick, R.: Momentum contrast for unsupervised visual representation learning. In: CVPR, 2020
32. He, K., Sun, J., Tang, X.: Single image haze removal using dark channel prior. TPAMI, 2010
33. Jha, D., Smedsrud, P.H., Riegler, M.A., Johansen, D., De Lange, T., Halvorsen, P., Johansen, H.D.: Resunet++: An advanced architecture for medical image segmentation. In: ISM, 2019
34. Jiang, K., Wang, Z., Yi, P., Chen, C., Lin, C.W.: Pcnnet: Progressive coupled network for real-time image deraining. In: TIP, 2021
35. Jin, Y., Sharma, A., Tan, R.T.: Dc-shadownet: Single-image hard and soft shadow removal using unsupervised domain-classifier guided network. In: ICCV, 2021
36. Kupyn, O., Martyniuk, T., Wu, J., Wang, Z.: Deblurgan-v2: Deblurring (orders-of-magnitude) faster and better. In: ICCV, 2019
37. Lee, H., Sohn, K., Min, D.: Unsupervised low-light image enhancement using bright channel prior. IEEE Signal Processing Letters, 2020
38. Levin, A., Weiss, Y., Durand, F., Freeman, W.T.: Understanding and evaluating blind deconvolution algorithms. In: CVPR, 2009
39. Li, L., Pan, J., Lai, W.S., Gao, C., Sang, N., Yang, M.H.: Blind image deblurring via deep discriminative priors. IJCV, 2019
40. Li, W., Lu, X., Lu, J., Zhang, X., Jia, J.: On efficient transformer and image pre-training for low-level vision. In: arXiv preprint 2112.10175
41. Li, X., Wu, J., Lin, Z., Liu, H., Zha, H.: Recurrent squeeze-and-excitation context aggregation net for single image deraining. In: ECCV, 2018

42. Li, X., Jin, X., Lin, J., Liu, S., Wu, Y., Yu, T., Zhou, W., Chen, Z.: Learning disentangled feature representation for hybrid-distorted image restoration. In: ECCV, 2020
43. Li, Y., Tan, R.T., Guo, X., Lu, J., Brown, M.S.: Rain streak removal using layer priors. In: CVPR, 2016
44. Liang, J., Cao, J., Sun, G., Zhang, K., Van Gool, L., Timofte, R.: Swinir: Image restoration using swin transformer. In: ICCVW, 2021
45. Liu, L., Liu, J., Yuan, S., Slabaugh, G., Leonardis, A., Zhou, W., Tian, Q.: Wavelet-based dual-branch network for image demoiréing. ECCV, 2020
46. Liu, L., Yuan, S., Liu, J., Guo, X., Yan, Y., Tian, Q.: Siamtrans: Zero-shot multi-frame image restoration with pre-trained siamese transformers (AAAI, 2022)
47. Liu, R., Yuan, Z., Liu, T., Xiong, Z.: End-to-end lane shape prediction with transformers. In: WACV, 2021
48. Liu, Y.F., Jaw, D.W., Huang, S.C., Hwang, J.N.: Desnownet: Context-aware deep network for snow removal. TIP, 2018
49. Liu, Z., Lin, Y., Cao, Y., Hu, H., Wei, Y., Zhang, Z., Lin, S., Guo, B.: Swin transformer: Hierarchical vision transformer using shifted windows. CVPR, 2021
50. Nah, S., Baik, S., Hong, S., Moon, G., Son, S., Timofte, R., Lee, K.M.: Ntire 2019 challenge on video deblurring and super-resolution: Dataset and study. In: CVPRW, 2019
51. Pan, J., Bai, H., Tang, J.: Cascaded deep video deblurring using temporal sharpness prior. In: CVPR, 2020
52. Pan, J., Sun, D., Pfister, H., Yang, M.H.: Blind image deblurring using dark channel prior. In: CVPR, 2016
53. Pan, X., Zhan, X., Dai, B., Lin, D., Loy, C.C., Luo, P.: Exploiting deep generative prior for versatile image restoration and manipulation. In: ECCV, 2020
54. Park, T., Efros, A.A., Zhang, R., Zhu, J.Y.: Contrastive learning for unpaired image-to-image translation. In: ECCV, 2020
55. Qian, R., Tan, R.T., Yang, W., Su, J., Liu, J.: Attentive generative adversarial network for raindrop removal from a single image. In: CVPR, 2018
56. Ren, D., Shang, W., Zhu, P., Hu, Q., Meng, D., Zuo, W.: Single image deraining using bilateral recurrent network. TIP, 2020
57. Ren, D., Zuo, W., Hu, Q., Zhu, P., Meng, D.: Progressive image deraining networks: A better and simpler baseline. In: CVPR, 2019
58. Richardson, E., Alaluf, Y., Patashnik, O., Nitzan, Y., Azar, Y., Shapiro, S., Cohen-Or, D.: Encoding in style: a stylegan encoder for image-to-image translation. arXiv preprint arXiv:2008.00951 (2020)
59. Ronneberger, O., Fischer, P., Brox, T.: U-net: Convolutional networks for biomedical image segmentation. In: MICCAI, 2015
60. Roth, S., Black, M.J.: Fields of experts: A framework for learning image priors. In: CVPR, 2005
61. Rudin, L.I., Osher, S., Fatemi, E.: Nonlinear total variation based noise removal algorithms. Physica D: nonlinear phenomena, 1992
62. Sun, Y., Yu, Y., Wang, W.: Moiré photo restoration using multiresolution convolutional neural networks. TIP, 2018
63. Ulyanov, D., Vedaldi, A., Lempitsky, V.: Deep image prior. In: CVPR, 2018
64. Vaswani, A., Shazeer, N., Parmar, N., Uszkoreit, J., Jones, L., Gomez, A.N., Kaiser, L., Polosukhin, I.: Attention is all you need. arXiv preprint arXiv:1706.03762, 2017
65. Wang, J., Li, X., Yang, J.: Stacked conditional generative adversarial networks for jointly learning shadow detection and shadow removal. CVPR, 2018

66. Wang, T., Yang, X., Xu, K., Chen, S., Zhang, Q., Lau, R.W.: Spatial attentive single-image deraining with a high quality real rain dataset. In: CVPR, 2019
67. Wang, X., Li, Y., Zhang, H., Shan, Y.: Towards real-world blind face restoration with generative facial prior. In: CVPR, 2021
68. Wang, Z., Cun, X., Bao, J., Liu, J.: Uformer: A general u-shaped transformer for image restoration. arXiv preprint 2106.03106
69. Yang, F., Yang, H., Fu, J., Lu, H., Guo, B.: Learning texture transformer network for image super-resolution. In: CVPR, 2020
70. Yang, S., Lei, Y., Xiong, S., Wang, W.: High resolution demoire network. In: ICIP, 2020
71. Yang, W., Tan, R.T., Feng, J., Liu, J., Guo, Z., Yan, S.: Deep joint rain detection and removal from a single image. In: CVPR, 2017
72. Yu, K., Dong, C., Lin, L., Loy, C.C.: Crafting a toolchain for image restoration by deep reinforcement learning. In: CVPR, 2018
73. Zeng, Y., Fu, J., Chao, H.: Learning joint spatial-temporal transformations for video inpainting. In: ECCV, 2020
74. Zhang, K., Zuo, W., Chen, Y., Meng, D., Zhang, L.: Beyond a gaussian denoiser: Residual learning of deep cnn for image denoising. TIP, 2017
75. Zhang, K., Zuo, W., Gu, S., Zhang, L.: Learning deep cnn denoiser prior for image restoration. In: CVPR, 2017
76. Zhang, K., Zuo, W., Zhang, L.: Ffdnet: Toward a fast and flexible solution for CNN based image denoising. TIP, 2018
77. Zhang, Y., Tian, Y., Kong, Y., Zhong, B., Fu, Y.: Residual dense network for image restoration. TPAMI, 2020
78. Zheng, B., Yuan, S., Slabaugh, G., Leonardis, A.: Image demoireing with learnable bandpass filters. In: CVPR, 2020
79. Zheng, B., Yuan, S., Yan, C., Tian, X., Zhang, J., Sun, Y., Liu, L., Leonardis, A., Slabaugh, G.: Learning frequency domain priors for image demoireing. TPAMI, 2021
80. Zhu, L., Fu, C.W., Lischinski, D., Heng, P.A.: Joint bi-layer optimization for single-image rain streak removal. In: ICCV, 2017
81. Zhu, Q., Mai, J., Shao, L.: A fast single image haze removal algorithm using color attenuation prior. TIP, 2015
82. Zhu, S.C., Mumford, D.: Prior learning and gibbs reaction-diffusion. TPAMI, 1997
83. Zhu, X., Su, W., Lu, L., Li, B., Wang, X., Dai, J.: Deformable detr: Deformable transformers for end-to-end object detection. In: ICLR, 2021

## A Comparison with general image restoration methods

We compare our TAPE-Net with two models, DnCNN [74] and UNet [59], which are widely used in image restoration tasks. As shown in Table S1, our model outperforms these two models by large margins on all datasets. Note that for a fair comparison, we set the compared models with a similar number of FLOPs. The parameters of DnCNN, UNet, and our TAPE are 0.5M, 9.8M, and 1.3M, respectively.

Table S1: Quantitative comparison for three models (in terms of PSNR (dB)).

Dataset	Rain200L	Rain200H	Raindrop800	SIDD	TIP2018	Snow100K	ISTD	FLOPs
DnCNN [74]	27.73	19.20	26.12	34.31	24.74	23.77	23.21	14.4 G
UNet [59]	31.50	22.50	26.41	33.72	25.58	23.48	25.64	18.2 G
TAPE-Net (Ours)	<b>33.17</b>	<b>23.84</b>	<b>27.69</b>	<b>37.90</b>	<b>27.52</b>	<b>26.33</b>	<b>26.57</b>	14.1 G

## B Comparison with denoising specific methods

As shown in Table S2, we compare our methods with state-of-the-art denoising methods (DnCNN [74], FFDNet [76], RDN [77], and SADNet [11]). Note that the FLOPs number of our method (14.1G) is much smaller than that of RDN (46.6G) or SADNet (45.8G), when the input is a  $64 \times 64$  RGB image. We replace our backbone model (original transformer) with a specially designed transformer, Swin transformer [49] (termed as ‘TAPE-Net-swin-L’ in Table S2), which outperforms all the SOTA methods with our 3-stage training.

Table S2: Quantitative comparison with the state-of-the-art denoising methods on SIDD.

Method	DnCNN [74]	FFDNet [76]	RDN [77]	SADNet [11]	TAPE-Net (Ours)	TAPE-Net-swin-L (Ours)
PSNR/SSIM	34.31/0.892	33.26/0.890	38.70/0.901	38.41/0.900	37.90/0.896	38.76/0.901
FLOPS (G)	14.4	0.87	46.6	45.8	14.1	5.3

## C Additional visualization results.

### C.1 Visualization some results of the prior queries, $Q$ .

We also visualize some other results of the prior queries ( $Q$ ) of TAPE. As shown in Fig. S1, (a) and (b) are rain inputs and ground truth respectively; (c) are one

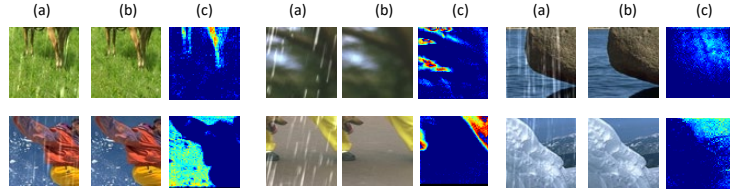


Fig. S1: Visualization of some results of the prior queries,  $Q$  on the Rain200L dataset. (a) Rain inputs. (b) Ground truth. (c) one of the predicted results of PLM.

of the predicted results of PLM. We can see that with the help of pre-training, the PLM module can correlate the information of similar textures or patches from a long distance. Thus, the transformer decoder of the backbone can utilize these long-distance similar areas/patches to restore the image.

## C.2 Visualization some results of learned parameters ( $e$ ).

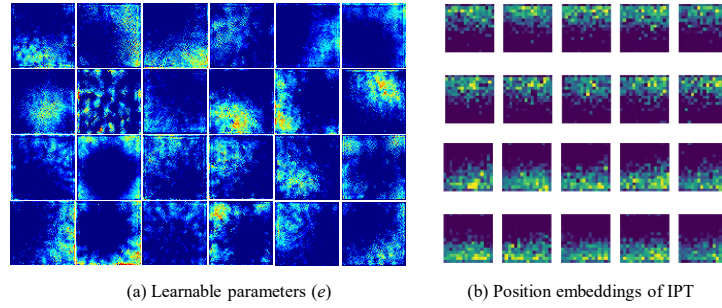


Fig. S2: Visual comparison between our learnable parameters and the position embeddings of IPT. Our learnable parameters show more richer patterns.

We visualize the learned parameters ( $e$ ) of TAPE. Fig. S2 shows some visualization results of learned parameters ( $e$ ) and the position embeddings of IPT (these results are copied from [12]). We can find that our learned parameters ( $e$ ) focus on other patches with farther distances than the position embeddings of IPT. Besides, our learned feature maps show richer patterns. For example, some of the patches focus on the four corners of the image at the same time (the patch on the 3rd row and 2nd column). Some of the patches focus on the characters of oblique directions (the patch on the 1st row and 5th column). These rich feature maps do not appear in the visualization results of IPT.

## D Additional results on other transformer backbones.

Our TAPE is a widely applicable method, where the backbone can be replaced by other transformer backbones. We replace our backbone network with the swin transformer backbone [49] for experiments. As shown in Table S3, ‘Baseline-swintrans’ is the Swin transformer backbone without pre-training. ‘TAPE-Net-swintrans-S’, ‘TAPE-Net-swintrans-M’, and ‘TAPE-Net-swintrans-L’ are our TAPE-Nets with the Swin transformer backbone and contain 1 Swin block, 3 Swin blocks and 5 Swin blocks, respectively. The results illustrate that our 3-stage pre-training and adding blocks can significantly boost the performance.

Table S3: Quantitative comparison for Baseline-swintrans and TAPE-Net-trans (in terms of PSNR (dB)). The numbers in () of the 2nd line are the PSNR gain compared with ‘Baseline-swintrans’.

	Blocks numbers	Network parameters	Rain200L (dB)	SIDD (dB)	Raindrop800 (dB)
Baseline-swintrans	1	0.19M	33.52	38.01	27.79
TAPE-Net-swintrans-S	1	0.19M	34.07 (+0.55)	38.76 (+0.75)	28.31 (+0.52)
TAPE-Net-swintrans-M	3	0.61M	34.20	38.87	28.97
TAPE-Net-swintrans-L	5	0.97M	34.46	38.98	29.15

## E Ablation Study about Transformer or CNN.

We replace the transformer encoder and decoder with the ResNet encoder and decoder [33] respectively with the same model size. The feature map outputted from the encoder and the feature map outputted from the PLM are concatenated and served as the input of the ResNet decoder. We do the ablation study on the Rain200L dataset with the same setting as Sec. 4.5 of the main paper. The PSNR/SSIM drops 1.03dB/0.006 compared with the baseline with the transformer encoder and decoder. The result shows that using the transformer is better when fusing the information of the output of PLM and the encoder. We also made a comparison between pre-trained CNN and no-pre-trained CNN. Compared with transformer, CNN’s performance improvement is much smaller.

## F Visual comparison with other SOTA methods on desnowing and shadow removal

We compare our method with several state-of-the-art desnowing and shadow removal methods. Fig. S3 and Fig. S4 show our method can remove the shadow or snow. Please note that these compared methods use the snow/shadow masks for training, while our method only uses snow/snow-free or shadow/shadow-free image pairs.

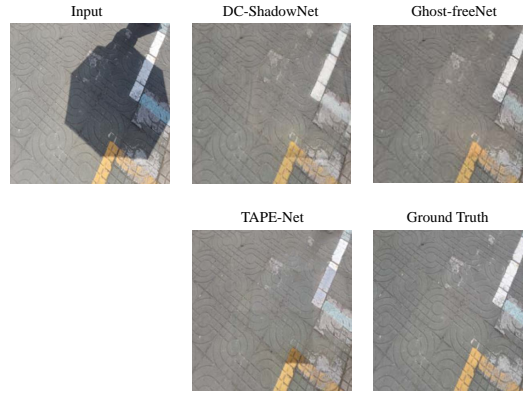


Fig. S3: Visual shadow removal comparison among ours and two other methods (DC-ShadowNet [35] and Ghost-freeNet [18]).

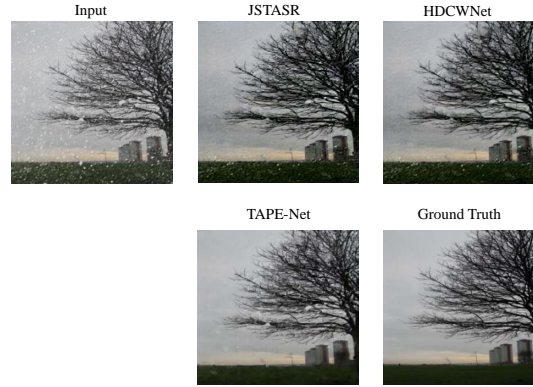


Fig. S4: Visual desnowing comparison among ours and two other methods (JSTASR [15] and HDCWNet [16]).